Available on CMS information server

CMS NOTE 2006/084

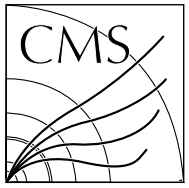

The Compact Muon Solenoid Experiment

CMS Note

Mailing address: CMS CERN, CH-1211 GENEVA 23, Switzerland

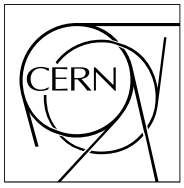

25 May 2006

Selection of single top events with the CMS detector at LHC

V. Abramov, D. Konstantinov, S. Slabospitsky

Institute for High Energy Physics, Protvino, Russia

M. Mohammadi Najafabadi

IPM and Sharif University of Technology, Tehran, Iran

A. Giammanco[a)], R. Tenchini

Istituto Nazionale di Fisica Nucleare, Pisa, Italy

E. Boos, L. Dudko, V. Savrin, A. Sherstnev[b)]

Skobeltsyn Institute of Nuclear Physics, Moscow State University, Moscow, Russia

S. Kalinin

Université Catholique de Louvain, Louvain-la-Neuve, Belgium

A. Drozdetskiy

University of Florida, Gainesville, USA

Abstract

The detection of single-top events with the CMS detector is discussed. Two selections are proposed, aimed to measure single top production in the Standard Model t- and s-channel, respectively. The perspectives of the measurements for an integrated luminosity of 10 fb^{-1} are described. The results are based on detailed detector simulations, either based on GEANT4, or on faster techniques. The reconstruction procedures developed by the CMS Collaboration are utilized.

[a)] Now at Université Catholique de Louvain, Louvain-la-Neuve, Belgium

[b)] Now at Cavendish Laboratory, University of Cambridge, UK

1 Introduction

In the Standard Model (SM) the top quark is a spin-$\frac{1}{2}$ fermion with electric charge $Q^t_{em} = \frac{2}{3} \mid e \mid$, the weak isospin partner of the b quark, and a color triplet. Even within the SM the top quark is a very special object. Indeed, the top quark is much heavier than all other quarks in the SM and the top Yukawa coupling is surprisingly close to one. The top quark lifetime, $\tau_t \approx 0.4 \times 10^{-24}$ s, is much smaller than the typical time for the formation of QCD bound states, $\tau_{\rm QCD} \approx 1/\Lambda_{\rm QCD} \approx 3 \times 10^{-24}$ s. Therefore, the top quark decays long before it can hadronize [1], providing a very clean source for fundamental information.

At the LHC the top quarks are expected to be produced either in pair or singly. Due to strong interactions of the top quarks with gluons the $t\bar{t}$-pair production mechanism dominates the top quark production rate. The NLO computations [2] including the re-summation of the Sudakov logarithms (NLL) [3] lead to top pair production cross section of about 830 pb. The electroweak single-top-quark production rate at the LHC is also calculated in the SM to the NLO level of accuracy for all three production mechanisms classified by the virtuality of the involved W-boson: t-channel ($q^2_W < 0$), s-channel ($q^2_W > 0$), and associated tW production ($q^2_W = M^2_W$), indicated by the Feynman diagrams in Fig.1. Since the LHC is a pp-collider, the cross sections for t and $\bar{t}$ production are not equal. The NLO cross sections are 152.6 pb and 90.0 pb for the t-channel t and $\bar{t}$ production respectively [4], and 6.55 pb and 4.07 pb for the s-channel t and $\bar{t}$ [5]. For the associated W production channel, the cross sections for t and $\bar{t}$ production are the same, giving for $W^-t + W^+\bar{t}$ about 60 pb [6].

The study of single top production provides a unique possibility to investigate many aspects of top quark physics, that cannot be easily studied in $t\bar{t}$ production. Some examples are:

- the direct measurement of V_{tb} (CKM matrix element);
- the investigation of the tWb vertex structure and of the FCNC $tu(c)g$ couplings directly in the production processes;
- the search for top anomalous couplings and s-channel resonances like W'-bosons.

Last but not least, single top quark production provides additional measurements of the top quark mass and of the top quark spin, supplementary to the top pair channel.

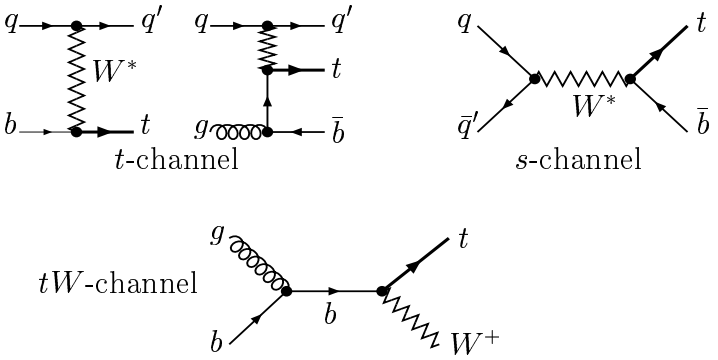

Figure 1: Representative diagrams, describing three channels of the single top production.

Realistic signatures and strategies to search for the single top will be specified in details in the following sections for the t-channel and s-channel production mechanisms. In general, the main problem in experimental studies of the single top processes is to find an optimal way to separate signal from backgrounds with rates much larger than the signal. The problem of background reduction is significantly more serious in single top selections comparing to the top pair case mainly because of the following reasons:

- smaller invariant mass ($\hat{s}$ threshold) and therefore much larger backgrounds which include contributions from larger gluon parton densities at smaller x in colliding protons;
- smaller number of final high p_T jets and therefore larger sensitivity to the $W^{\pm}$+ jets background;
- top pair production itself, giving a significant background contribution.

A priori, the most dangerous background comes from multi-jet QCD events, but such background can be reduced substantially by considering only leptonic decays of the $W^{\pm}$-bosons from top-quark decays. Therefore in this study for both t- and s-channel production, final states with one isolated charged lepton (muon or electron) are used. This signature is supplemented by the requirement of missing energy, one or two jets from b-quark (b-jets) and one or zero "forward" hadronic light jet.

The paper is organized as follows. In the next section some details are given about the generation of signal and background samples. In Section 3, results are shown for the selection of t-channel events. In Section 4, results are shown for the s-channel.

2 Details on the signal and background generation

Two generators, SingleTop [8] (based on the CompHEP package [9]) and TopReX [10] were used to generate events for all three single top production processes. These generators reproduce correctly the NLO distributions; spin correlations, finite W-boson and t-quark widths, and non-zero b-quark mass have been taken into account. (Details for the matching procedure are given in Ref. [8]).

The background processes, namely $Wb\bar{b}$, $Wb\bar{b}+j$ and $W+2j$, were generated with the CompHEP, TopReX, and MadGraph [11] programs as indicated in Table 1. The hard process events containing all needed information were then passed to PYTHIA 6.227 [12] for showering, hadronization and decays of unstable particles. The $t\bar{t}$ and $W+j$ background events were generated by means of the same PYTHIA version.

In the event samples for the single top signal and the $Wb\bar{b}$ and $W+jets$ backgrounds the leptonic decay modes into e, μ, τ of W-bosons were considered. For the $t\bar{t}$ background events not only leptonic but also hadronic W-boson decay modes were used in order to take into account events with leptons originated from b-quark decays. For $Wb\bar{b}$ this was not taken into account yet, however the corresponding correction is expected to be small.

The list of the signal and background process cross sections as well as generators used are given in the Table 1. The following parameters were used for all computations: $M_t = 175$ GeV/c^2, $\Gamma_t = 1.55$ GeV/c^2, $M_W = 80.4$ GeV/c^2, $\Gamma_W = 2.04$ GeV/c^2, $M_b = 4.7$ GeV/c^2. In this study, the cross section of the $W(\rightarrow \mu)b\bar{b}+j$ and $W(\rightarrow \mu)+2j$ processes are defined with the following kinematic constraints: $P_T(\mu) > 17$ GeV/c, $|\eta(\mu)| < 2.2$, $P_T(j) > 20$ GeV/c, $|\eta(j)| < 5.0$, $\Delta R(j,j) = \sqrt{(\Delta\eta)^2 + (\Delta\phi)^2} > 0.5$, and corresponding cuts were applied.

Table 1: Cross sections and generators for the signal and background processes

Process	σ, pb	generator
t-channel	245 (NLO)	SingleTop, TopReX
tW-channel	60 (NLO)	TopReX
s-channel	10 (NLO)	TopReX
$t\bar{t}$ (inclusive)	833 (NLO)	PYTHIA
Wbb	300 (LO)	TopReX
$Wbb+j$	32.4 (LO)	MadGraph
$W+j$	9660 (LO)	PYTHIA
$W+2j$	987 (LO)	CompHEP, AlpGen

To improve the efficiency of the t-channel event generation a kinematic preselection was used:

- $P_T(\mu) > 9$ GeV/c and $|\eta(\mu)| < 2.4$
- $P_T(j) > 10$ GeV/c, $|\eta(j)| < 5.0$, $\Delta R(j,j) > 0.5$

These cuts allow to generate the signal events only in the kinematical region exploited in the current analysis. The resulting cross-section for t-channel, after these cuts, is σ(t-channel) = 180 pb. No trigger cuts are applied at this stage.

The CMS full detector simulation was performed with OSCAR [13] and ORCA [14]. The version OSCAR_3_6_5 was used in order to prepare Hits, ORCA_8_7_1 [14] was used to prepare Digis (Digis were mixed with the Pile-up events corresponding to an instantaneous luminosity of $1.2 \times 10^{33}\mathrm{cm}^{-2}\mathrm{s}^{-1}$, produced officially by CMS), ORCA_8_13_1 was used to prepare DST's. FAMOS [15] (a program for fast simulation of the CMS detector) was used for s-channel events, as described in Sec. 4.

A brief description of the reconstruction algorithms utilised in the present study is given below.

The muons are reconstructed by using the standard CMS algorithm combining tracker and muon chamber information as described in Ref. [16], and tracker and calorimeter isolation cuts are applied, as described in Ref. [17]. The electrons are reconstructed by the standard CMS algorithm combining tracker and ECAL informations, see Ref. [18].

The jets are reconstructed by the Iterative Cone algorithm with the cone size of 0.5 (Ref. [19]) and for the calibration both the Monte Carlo (in the t-channel analysis) and the $\gamma + jets$ (in the s-channel) methods are used (Ref. [20]). For b-tagging a probability algorithm based on the impact parameter of the tracks is used, as described in Ref. [21].

The transverse missing energy is defined by using the following equation:

$$\vec{\not{E}}_{\mathrm{T}} = -\left(\sum \vec{E}_T^{tower} + \sum(\vec{E}_{T,jet}^{calib}) - \sum(\vec{E}_{T,jet}^{raw})\right) \quad (1)$$

where E_T^{tower} is the sum of transverse energy of towers, $E_{T,jet}^{calib}$ ($E_{T,jet}^{raw}$) is the transverse energy of calibrated (raw) jets.

3 Single-top production in t-channel

3.1 Particle distributions at the partonic level

Transverse momentum (p_T) and pseudorapidity (η) distributions at generator level are presented on Figs. 2 and 3 for signal events.

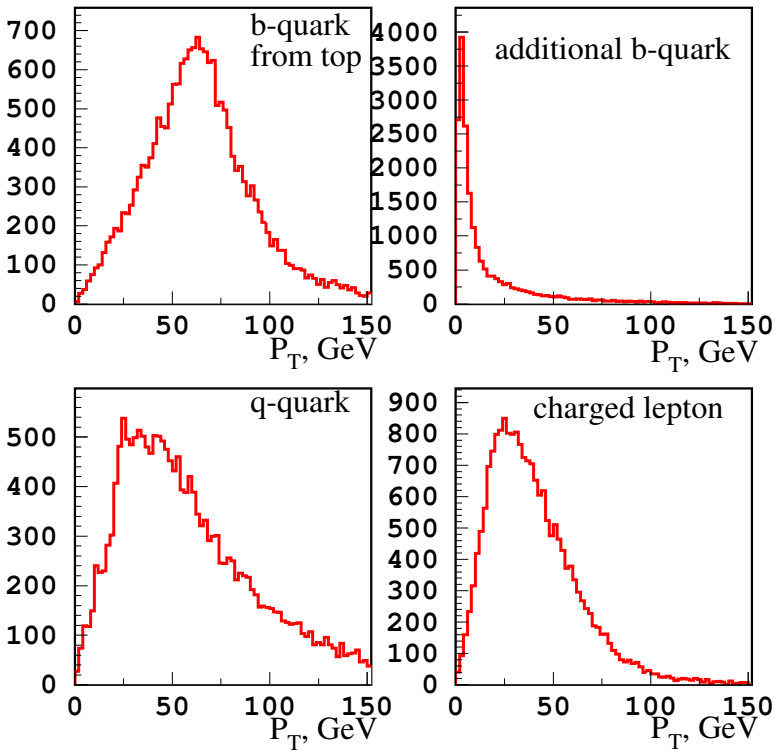

Figure 2: Transverse momentum distributions of the final b-quarks, the light forward quark and charged lepton at the partonic level in signal events generated with SingleTop.

As shown by Fig. 2 the b-quark from top-quark decay, the charged lepton and the light quark have relatively large transverse momenta and will be reliably reconstructed by the CMS detector. The additional b-quark, however, is produced with small transverse momentum, making the reconstruction of the associated low-p_T jet, and its b-tagging, very difficult. Therefore, only two hadronic jets in the final state are required and only the muonic decay of the top is considered.

A second specific feature of single top events is the production of a light jet in the forward/backward direction (see Figs. 3). Therefore, a cut on the pseudorapidity of a such jet (i.e. $|\eta_j| > 2.5$) is very useful for background suppression.

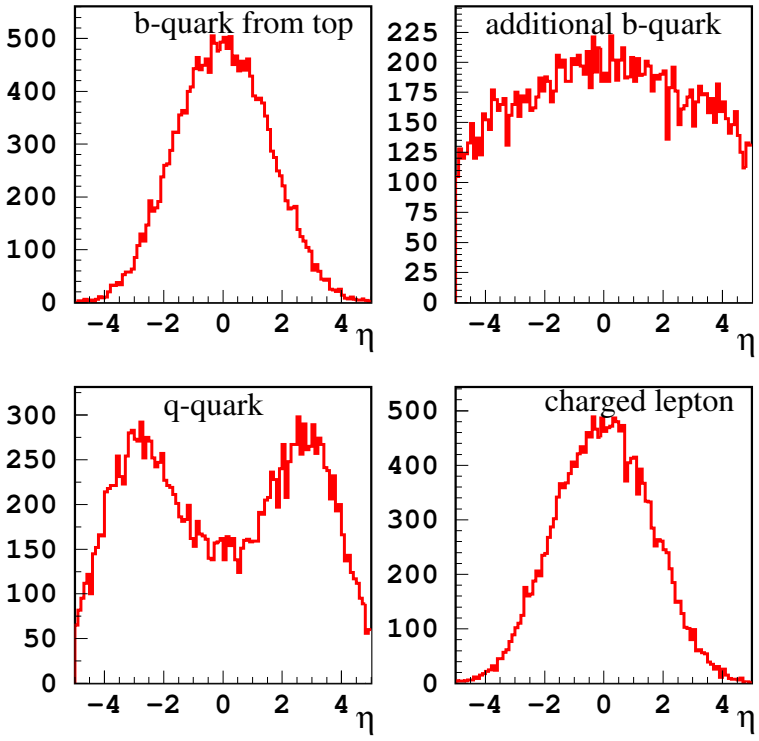

Figure 3: Pseudorapidity distributions of the b-quarks, the light forward quark and charged lepton at the partonic level in signal events generated with SingleTop.

3.2 Analysis of the fully simulated events

The variables used for signal/background separation are introduced in this section.

The histogram of the number of jets for the signal (the solid curve) and the background events is shown on the left part of Fig. 4. The pseudorapidity distribution of the light jet is shown on the right part of Fig. 4. From these figures one can see a clear difference between signal and background events. In particular, the usefulness of requiring a non-b-tagged jet at high η, suggested by the study at generator level, is confirmed.

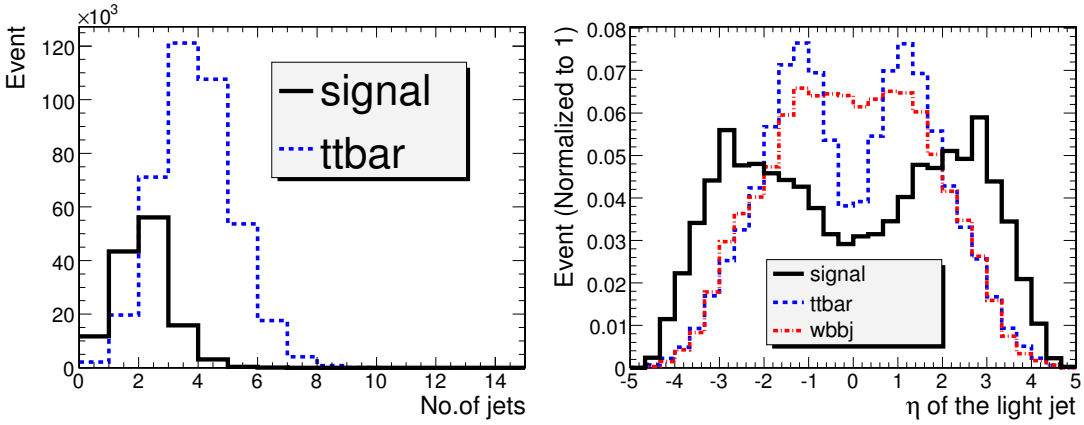

Figure 4: Numbers of jets with $p_T > 20$ GeV/c (left). Pseudorapidity (η) of the light jet (right).

In order to reconstruct the W-boson momentum, one needs to know the transverse ($P_{T,\nu}$) and longitudinal ($P_{z,\nu}$) components of the ν momentum. The transverse missing energy ($\not\!\!E_{\rm T}$) is taken as a measurement of ($P_{T,\nu}$). Substantial differences are seen (Fig. 5) between the reconstructed missing transverse energy and the 'true' neutrino. The $P_{z,\nu}$ component is extracted from the quadratic equation:

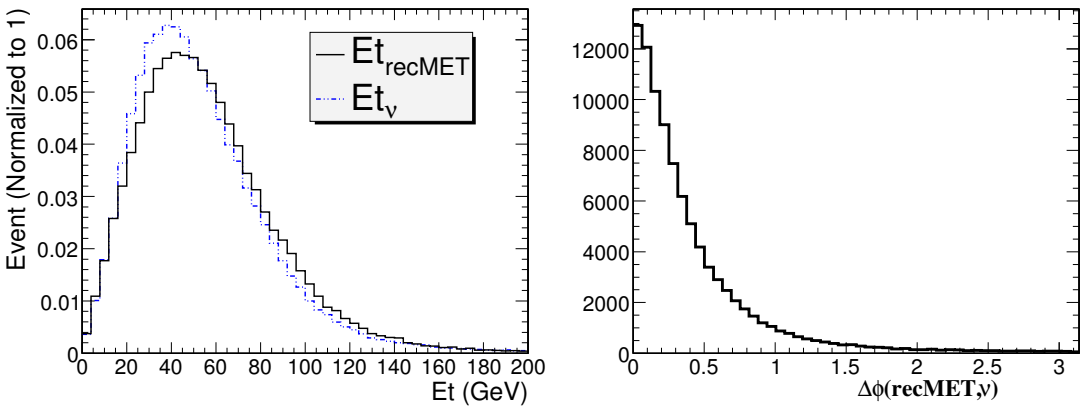

Figure 5: Missing transverse energy and transverse component of neutrino (left). Angular difference between reconstructed $\not\!\!E_{\mathrm{T}}$ and neutrino in transverse plane (right).

$$M_W^2 = 2\left(E_\mu\sqrt{P_{z,\nu}^2 + \not\!\!E_{\mathrm{T}}^2} - \vec{P}_{T,\mu}\cdot\vec{\not\!\!E}_{\mathrm{T}} - P_{z,\mu}P_{z,\nu}\right) \tag{2}$$

This equation has two solutions:

$$P_{z,\nu}^{(1,2)} = \frac{AP_{z,\mu} \pm \sqrt{\Delta}}{P_{T,\mu}^2} \tag{3}$$

where $A = \frac{M_W^2}{2} + \vec{P}_{T,\mu}\cdot\vec{\not\!\!E}_{\mathrm{T}}$ and $\Delta = E_\mu^2(A^2 - \not\!\!E_{\mathrm{T}}^2 P_{T,\mu}^2)$.

Among the two solutions of Eq. 2 the minimal value of the $|P_{z,\nu}|$ is used for W-boson momentum reconstruction. In about 30% of the events Δ has negative values and therefore Eq. 2 has no solutions. This is due to the finite detector resolution, mainly for the hadronic calorimeter HCAL, and to the presence of extra missing energy in the event (neutrinos from meson decays and particles outside acceptance), as mentioned in Section 4.2. In this case the parameter M_W is increased until Δ becomes non-negative(i.e. $\Delta = 0$). Using this new value of M_W, $P_{z,\nu}$ is calculated from Eq. 3.

For further signal/background separation two specific kinematic variables are introduced:

$$\vec{\Sigma}_T \equiv \vec{P}_T(W) + \vec{E}_T(b\,\text{jet}) + \vec{E}_T(\text{light jet})\ \ [+\vec{E}_T(\text{second } b\,\text{jet})], \tag{4}$$

$$M_T^W = \sqrt{2(P_{T,\mu}\not\!\!E_{\mathrm{T}} - \vec{P}_{T,\mu}\cdot\vec{\not\!\!E}_{\mathrm{T}})}. \tag{5}$$

The first variable, $\vec{\Sigma}_T$, is the vector sum of transverse momenta of all the final reconstructed objects (jets, muon and $\not\!\!E_{\mathrm{T}}$) expected for the signal case, while M_T^W is transverse mass of the W-boson. At the partonic level $|\vec{\Sigma}_T|$ equals zero for signal. Figure 6 shows this variable for signal and $t\bar{t}$ background after full simulation and reconstruction.

3.3 Kinematical cuts used for analysis

At the beginning the following requirements on the final-state muon are applied: only one isolated muon with $p_T > 19$ GeV/c and $|\eta_\mu| < 2.1$. These cuts reproduce the HLT selection.

Then, two pre-selection cuts are used:

- transverse missing energy, $\not\!\!E_{\mathrm{T}} > 40$ GeV;
- at least two hadronic jets, with transverse momenta (uncalibrated) $p_T > 20$ GeV/c.

For the t-channel analysis the combined b-tagging algorithm is used [21] and the Monte-Carlo calibrations for hadronic jets are applied.

Before proceeding to the cut's optimization procedure the following additional requirements are used:

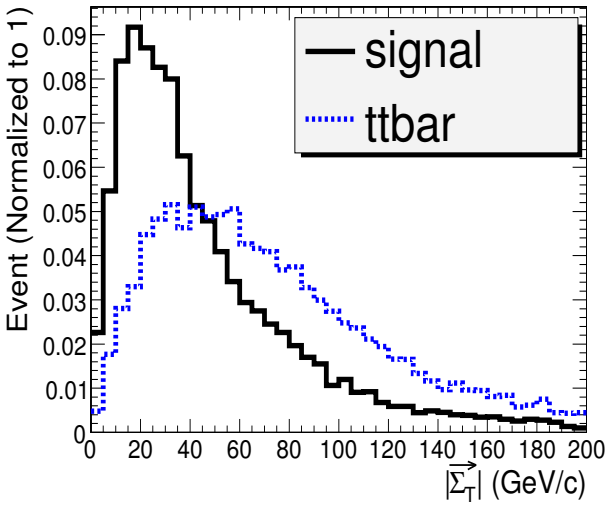

Figure 6: $|\vec{\Sigma}_T|$.

- a W-boson is reconstructed with the minimal value of the $|P_{z,\,\nu}|$ as discussed in Sec. 3.5;
- at least one of the selected jets should have the b-tag discriminator (defined as in [21]) larger than 2.4 and $|\eta(B)| < 2.5$;
- the second (light) jet should be in the forward region, i.e. $|\eta(L)| > 2.5$;
- jet veto: only two jets (calibrated) with $p_T^{calib} \geq 35$ GeV/c and no other hadronic jets with $p_T^{calib} \geq 35$ GeV/c;
- a top candidate is reconstructed from the W-boson and the "b-jet".

3.4 Search optimization by Genetic Algorithm methods

The specific kinematical features of the signal, like the number of jets, the vector sum of the transverse momentum of the final objects, and the transverse mass of the W-boson, are used for suppression of background events. The selection strategy explores the cuts in different kinematical ranges in order to obtain good signal-to-background ratio and large significance. The final optimizations of the cuts was done by using the Genetic Algorithm for Rectangular Cuts OptimizatioN (GARCON) program [26], which exploits mechanisms that have analogy in biological evolution: breeding, mutation, collapse of the population, etc. Environment requirements select at each step of "evolution" the best individual. In our case it is a requirement to have a cut values set which leads to the largest possible value for a "quality function", while keeping a reasonable number of signal events.

Genetic algorithms are very useful for maximization problems with a large number of discrete solutions or in other words for cuts optimization problems, for which we often have a huge number of possible sets of cut values. GARCON tries effectively 40^{24} cut sets in a few hours on event samples of the order of 10^5 events. One can look at some optimization examples listed in [26].

3.5 Analysis of the fully simulated events for 10 fb^{-1}

In this study (dedicated to 10 fb^{-1} integrated luminosity) for the optimization the following variables are used: $\not{E}_{\rm T}$, number of jets, $E_T(\mu)$, $E_T(Ljet)$, $E_T(Bjet)$, b-tag discriminator of the b-jet, $|\vec{\Sigma}_T|$. As optimization function, the signal-over-background ratio times significance is chosen.

The optimization with GARCON yielded the following cut values:

- $\not{E}_{\rm T} > 40.0$ GeV;
- Muon: $p_T(\mu) > 19.0$ GeV/c and $|\eta_(\mu)|$: (-2.1,2.1);
- b-jet: $p_T > 35.0$ GeV/c, $|\eta| < 2.5$ and Discriminator > 2.4;

- L-jet: $p_T > 40.0$ GeV/c and $|\eta| > 2.5$;
- $|\vec{\Sigma}_T|$ cut window: $(0.0, 43.5)$ GeV/c
- $50 < M_T^W < 120$ GeV/c^2
- top mass window: 110 GeV $< M_{\rm rec}(top) < 210$ GeV/c^2

The resulting efficiencies after application of cuts and the resulting number of events are given in the Table 2. The cumulative efficiency of any cut is defined as the ratio of events after application of all the cuts up to that row over the initial number of events.

Table 2: Number of events and cumulative efficiencies for each cut used in the analysis of t-channel single top production for 10 fb^{-1}. The symbol "$p_{TB} \times p_{Tj} \times \not{E}_{\rm T}$" means: $p_{TB} > 35$ GeV/c, $p_{Tj} > 40$ GeV/c, $|\eta_j| > 2.5$, $\not{E}_{\rm T} > 40$ GeV. The difference in efficiencies after the "isolated muon" cut is due to different decay modes of the W-boson: $t\bar{t}$ - all W decay channels, $W + j$ - three leptonic modes ($W \to e, \mu, \tau$), $W + b\bar{b}j$ and $W + 2j$ - only decay to muon.

	signal	$t\bar{t}$	$W(\to \mu)b\bar{b}j$	$W(\to e, \mu, \tau)j$	$W(\to \mu)jj$
N(events) at 10 fb^{-1}	1.8×10^5	8.33×10^6	3.24×10^5	9.7×10^7	9.9×10^5
isolated muon	0.73	0.14	0.52	0.16	0.81
$p_{TB} \times p_{Tj} \times \not{E}_{\rm T}$	0.036	6.4×10^{-3}	3.4×10^{-3}	9×10^{-6}	3×10^{-3}
veto on 3^{rd} jet	0.021	5.8×10^{-4}	1.6×10^{-3}	4×10^{-6}	1.1×10^{-3}
$0.0 < \Sigma_T < 43.5$ GeV/c	0.018	4.1×10^{-4}	1.2×10^{-3}	4×10^{-6}	6.8×10^{-4}
$50. < M_T^W < 120$ GeV/c^2	0.015	2.2×10^{-4}	9.6×10^{-4}	1×10^{-6}	5.4×10^{-4}
$110 < M_{\rm rec}(top) < 210$ GeV/c^2	0.013	1.4×10^{-4}	5.8×10^{-4}	0	4.1×10^{-4}
Number of events	2389	1188	195	0	402

A special treatment is required for the background due to QCD-jets, due to its huge cross section. The currently available DSTs have very small statistics. Typically each sample consists of $\sim$ 100K events, while the the expected numer of event for 10 fb^{-1} luminosity is about 10^{11} (Table 3). Moreover, no events remain after the application of the pre-selection cuts. Therefore, in order to roughly estimate the impact of the QCD-background, the cuts are applied separately, assuming they are uncorrelated. The results are given in Table 3. The requirement to have one isolated muon leads to a suppression factor of about $\epsilon_\ell = \mathcal{O}(10^{-4})$. The second requirement is $\not{E}_{\rm T} > 40$ GeV and only two jets (one b-jet and one light forward jet). This cut leads to a suppression of about $\epsilon_J = 10^{-4} - 10^{-3}$ depending on the $\hat{k}_T$ range. It was found that contributions from higher $\hat{k}_T$-range (i.e. $\hat{k}_T > 800$ GeV/c gives negligible contribution).

Table 3: Cross sections and number of events for 10 fb^{-1} for QCD-jets. The suppression factors for QCD-background are computed after the separate application of the pre-selection cuts: one isolated muon (ϵ_ℓ) and two hadronic jets plus missing transverse energy (ϵ_J). $N(\ell + J + \not{E}_{\rm T})$ is the number of events expected after application of these two cuts, assuming them to be uncorrelated.

$\hat{k}_T$-range, GeV/c	X-section	$N_{\rm ev}$ at 10 fb^{-1}	ϵ_ℓ	ϵ_J	$N(\ell + J + \not{E}_{\rm T})$
50-80	20 μb	2×10^{11}	1×10^{-4}	2×10^{-5}	400
80-120	2.96 μb	3×10^{10}	2.6×10^{-4}	1.7×10^{-4}	1300
120-170	498 nb	5×10^9	5×10^{-4}	1.4×10^{-3}	3500
170-230	100 nb	1×10^9	3.2×10^{-4}	2.6×10^{-3}	830
230-300	24 nb	2.4×10^8	9×10^{-4}	4×10^{-3}	820
300-380	6.4 nb	6.4×10^7	3.7×10^{-4}	1.6×10^{-3}	38
380-470	1.8 nb	1.8×10^7	1.2×10^{-3}	$1. \times 10^{-3}$	22
470-600	690 pb	6.9×10^6	4.2×10^{-3}	$4. \times 10^{-4}$	11
600-800	202 pb	2.0×10^6	3.6×10^{-3}	$4. \times 10^{-4}$	3
50-800					6924

After the application of both cuts (i.e. $\epsilon_\ell \times \epsilon_J$) the QCD-background gives a rather small contribution in comparison with the other backgrounds considered in this note as well as to the signal:

$$N_{\rm QCD} = 6924, \quad N_{\rm bckg} = 8.9 \times 10^4, \quad \Rightarrow \frac{N_{\rm QCD}}{N_{\rm bckg}} = \frac{6924}{8.9 \times 10^4} = 0.078$$

Therefore, one may conclude that QCD background will give a very small contribution to other background processes (less than 8%) and it will not be considered in the following.

The resulting signal-to-background ratio and the significance are as follows (for 10 fb^{-1}):

$$\frac{N_S}{N_B} = 1.34, \quad S_{stat} = \frac{N_S}{\sqrt{N_S + N_B}} = 37. \tag{6}$$

The final distribution on the reconstructed top mass is shown in Fig. 7. It is seen that such cuts provide a satisfactory background suppression.

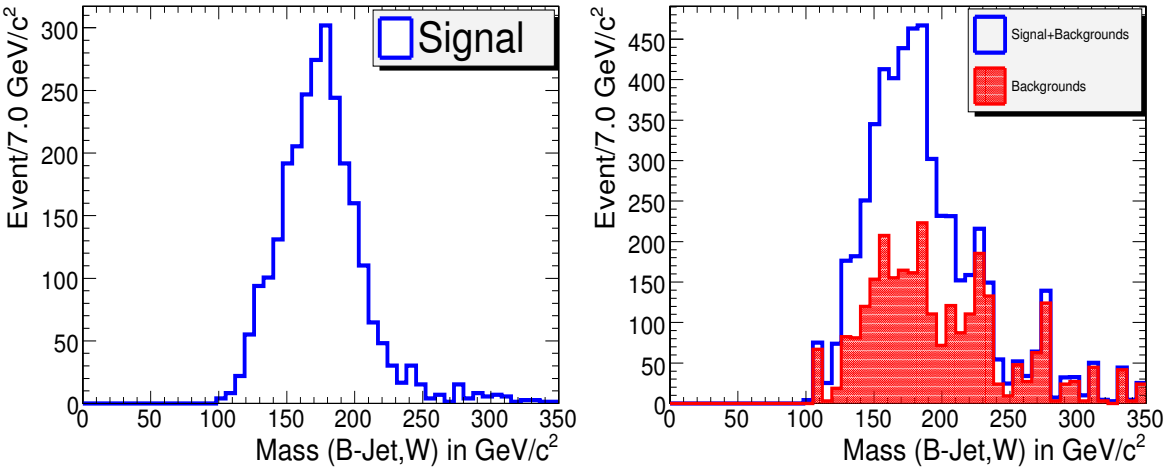

Figure 7: The distribution on the reconstructed top mass, for signal only (left) and with background included (right).

3.6 Systematic uncertainties

Three sources of the systematic errors are considered.

The theoretical errors to the total rate of the signal are calculated in detail in [23], and they consist of

- the PDF uncertainties: $+1.3\%, -2.2\%$,
- the higher orders (QCD scale): 3%,
- the variation of the top mass within 2 GeV$/c^2$: $+1.56\%, -1.46\%$,
- the uncertainty on the b-quark mass: $< 1\%$.

A sum in quadrature leads to the total theoretical uncertainty:

$$\Delta_{\rm th} = +3.6\%, \ -4.0\% \ \approx \pm 4\% \tag{7}$$

The theoretical uncertainties in the background events are assumed to be: 5% for $t\bar{t}$ [27], 17% for $Wb\bar{b}j$, 7% for $W + j$, 5% for Wjj [28].

The most relevant detector systematics are expected to be the uncertainties on the jet energy scale and on the b-tagging efficiency. The uncertainty due to jet energy measurement (JES) is expected to be 5% for jets with $p_T \approx 25$ GeV$/c$ and 2.5% with $p_T \approx 50$ GeV$/c$ with a linear dependence inside this range [29]. The b-tagging

Table 4: Number of selected events at 10 fb^{-1} with uncertainties due to different sources. An uncertainty of 5% comes from luminosity, 4% from b-tag. The theoretical uncertainty of 4% is assumed for the signal events, 5% for $t\bar{t}$, 17% for $Wb\bar{b}j$, and 5% for Wjj events. Here $\Delta N_{\rm syst}$ is sum in quadrature the theoretical, JES and b-tagging uncertainties, while $\Delta N_{\rm tot}$ includes also the luminosity uncertainty. The last column ($\Delta N_{\rm stat}$) shows the expected statistical uncertainty at 10 fb^{-1}.

sample	selected	ΔN_{th}	JES	$\Delta N_{\rm b-tag}$	$\Delta N_{\rm syst}$	$\Delta N_{\rm Lum}$	ΔN_{tot}	$\Delta N_{\rm stat}$
t-channel	2389	96	71	96	153	119	194	49
$t\bar{t}$	1188	59	73	48	105	59	121	34
$Wb\bar{b}j$	195	33	6	8	35	10	36	14
Wjj	402	20	0	16	26	20	33	20

uncertainty is taken as $\pm 4\%$ [30]. The uncertainty due to luminosity is expected to be 5% [24]. All these systematic uncertainties, evaluated for 10 fb^{-1}, are given in Table 4.

The statistical error is computed as

$$\frac{\Delta\sigma_{stat}}{\sigma} = \frac{\sqrt{N_S + N_B}}{N_S} = 2.7\%, \tag{8}$$

while the systematic error is taken as

$$\frac{\Delta\sigma_{syst}}{\sigma} = \frac{\Delta N_S \oplus \Delta N_B}{N_S} = 8.0\%, \tag{9}$$

where ΔN_S and ΔN_B are the quadratic sums, for signal and backgrounds respectively, of the errors quoted in Table 4 (with the exception of the luminosity uncertainty).

The total error, including also the 5% luminosity uncertainty, is

$$\frac{\Delta\sigma}{\sigma} = \frac{\Delta\sigma_{stat}}{\sigma} \oplus \frac{\Delta\sigma_{syst}}{\sigma} \oplus \frac{\Delta L}{L} = 10.1\%. \tag{10}$$

4 Single-top production in s-channel

The study of single top production via the s-channel process $q\bar{q'} \to W^* \to t\bar{b}$ ($\bar{t}b$) [23] gives a complementary measurement of the $|V_{tb}|$ CKM matrix element, due to the completely different initial state, with respect to the t-channel mode. This involves only u ($\bar{u}$) and d ($\bar{d}$) quarks, whose PDF's are the best known, while the t-channel and Wt associated productions include the less known gluon and b ($\bar{b}$) quark PDF's. Moreover, it is possible to extract $|V_{tb}|$ from the ratio $\sigma(q\bar{q'} \to W^* \to t\bar{b}\,(\bar{t}b))/\sigma(q\bar{q'} \to W \to \mu\nu)$, which cancels the PDF dependence. (Of course this will require some care, since the selection cuts may introduce a dependence in the ratio if they select different phase spaces for the tb and the $\mu\nu$ systems.)

An additional reason of interest on the s-channel production cross section is its sensitivity to the existence of additional bosons, e.g. Kaluza Klein excitations of the W or high mass $H^{\pm}$ [25].

For this study FAMOS_1_4_0 was used for fast detector simulation, applied to generator level samples generated as in Sec. 2, with pile-up corresponding to the design luminosity (for the LHC "low luminosity" phase) of $2 \times 10^{33}\ cm^{-2}s^{-1}$. The number of events used is listed in Table 5.

4.1 High Level Trigger selection

The present analysis is based on leptonic channels, i.e. the top is identified and reconstructed by its semileptonic decays into $l\nu b$ final states, with $l = e, \mu$. So, the signal will be looked for in events for which the single lepton triggers fired.

Here the HLT p_T thresholds from the CMS DAQ-TDR [22] are assumed: 19 GeV/c for the single muon and 29 GeV/c for the single electron; the allowed angular ranges are $|\eta| \leq 2.1$ for muons, $|\eta| \leq 2.4$ for electrons. The effect of these selections is shown in table 6. The dilepton triggers are not used since the signal is expected to have only one hard lepton, while some important backgrounds have two (e.g. $t\bar{t} \to l\nu bl\nu b$, $Zb\bar{b}$). The single-jet trigger [22] has a very high threshold, unfit to the spectra of jets from top decay (p_T >657 GeV/c, while the mass

Table 5: Cross sections, generators and number of events simulated with FAMOS for the signal and background processes.

Process (decay channel)	$\sigma \times Br$, pb	generator	n. of simulated events
s-channel ($W \to e, \mu, \tau$)	3.3 (NLO)	TopReX	233.000
t-channel ($W \to e, \mu, \tau$)	81.7 (NLO)	TopReX	690.000
$t\bar{t}$ ($W \to$ anything)	833 (NLO)	PYTHIA	2.760.000
Wt (2 $W \to e, \mu, \tau$)	6.7 (NLO)	TopReX	100.000
Wt (1 $W \to e, \mu, \tau$)	33.3 (NLO)	TopReX	157.000
$Wb\bar{b}$ ($W \to e, \mu, \tau$)	100 (LO)	TopReX	549.000
$W + 2j$ ($W \to e, \mu, \tau$)	2500 (LO)	AlpGen	461.000
$Z(/\gamma^*)b\bar{b}$ ($Z/\gamma^* \to \mu^+\mu^-$)	116 (LO)	CompHEP	59.000

difference between the top and the W plus the b is around 90 GeV/c only), and the same holds for the three- and four-jet triggers (p_T >247 GeV/c and 113 GeV/c respectively), which would anyway select much more $t\bar{t}$ background than signal. Also the combined trigger for jet and $\not{E}_{\mathrm{T}}$ has thresholds too high for the single top case: 180 GeV/c for the jet, 123 GeV/c for the missing energy.

Since this production mode suffers from low statistics, one could envisage the introduction of a combined trigger $e \times jet$, with threshold 19 GeV/c for the electron (in order to make the electronic sample more coherent with the muonic sample) and 45 GeV/c for the jet. This value has been chosen to be the same as the threshold for the τ-jet in the already existing $e \times \tau - jet$ trigger. It also corresponds to roughly one half of the kinetic energy available to the decay products in the rest frame of the top quark. Of course a detailed optimization of this threshold against the QCD background is required. The number of events that can be recovered this way in the $19 < p_T^e < 29$ GeV/c range, compared to the efficiencies of the two single lepton triggers, is shown in table 6.

Trigger	s-ch. ($W \to l\nu$)	t-ch. ($W \to l\nu$)	$t\bar{t}$ (inclusive)	Wbb ($W \to l\nu$)	Zbb ($Z \to \mu^+\mu^-$)
1μ	23.9%	25.4%	21.0%	17.3%	24.5%
$1e$	24.9%	25.5%	36.0%	13.7%	0.4%
$e \times j$	7.0%	7.0%	16.0%	0.7%	0.1%

Table 6: Fraction of events selected by the single-muon, single-electron and electron plus jet triggers, for signal and some representative backgrounds.

4.2 Preselection

The selection strategy can be summarized as a preselection followed by tight cuts on several discriminating variables, with thresholds optimized with a Genetic Algorithm technique.

The preselection is as follows:

- The event has to fire at least one of the triggers envisaged in Section 4.1 (including the proposed $e \times j$).
- The event must contain one lepton (e, μ) with $p_T \geq 19$ GeV/c and no other lepton above 10 GeV/c; the angular region allowed is $|\eta| \leq 2.1$ for muons, $|\eta| \leq 2.4$ for electrons.
- Exactly two jets must have $p_T \geq 30$ GeV/c and no other jet has to be present with $p_T \geq 20$ GeV/c (here the jet momenta are considered uncalibrated, and the angular region taken into account is $|\eta| \leq 3.0$). Jets matched to less than two charged tracks are ignored in this counting.
- The lepton has to be isolated. The isolation criterion chosen in this analysis is to sum the p_T of all the tracks in a cone of $\Delta R < 0.2$ around the lepton track, and to reject the event if this sum is greater than 5% of the lepton p_T. It has to be noted that, in the electron case, all the momentum components have been rescaled by E/p, with E measured by ECAL and p by the curvature of the electron track.
- Both jets should have a positive b-tagging discriminator value.
- The event should have a transverse missing energy $\not{E}_{\mathrm{T}}$ greater than 30 GeV.
- The lepton and the missing energy combined together have to form a transverse mass less than 100 GeV/c^2.

A W mass constraint is applied in order to extract the longitudinal component of the neutrino, as described in Sect. 3.5. If the solutions of Eq. 2 are real then the one giving the smallest $|P_{z,\nu}|$ is used (see Sec. 3.5). Differently from Sect. 3.5, the criterion chosen for this analysis if they are complex is to use only the real part of $P_{z,\nu}$ (assuming that the imaginary component only comes from resolution effects).

This is justified by Fig. 8, showing the variable Δ as defined in Eq. 3 using different $\not\!\!E_{\rm T}$ definitions for illustration purposes. In Fig. 8a, the true neutrino transverse momentum is used inside the W mass constraint equation (Eq. 2). In Fig. 8b it is replaced by the vectorial sum of all the invisible transverse momenta at generator level, showing how this affects the fraction of events that don't give real solutions. At last, Fig. 8c is obtained with the realistic $\not\!\!E_{\rm T}$ (as used in the analysis), including all the detector effects in a realistic LHC environment (i.e. including pile-up). In the three histograms Δ is progressively smeared, but most of the events with $\Delta < 0$ are still very close to the peak. The requirement of giving real solutions to eq. 3 may be safely loosened allowing for those small negative values, and the rejection of events clearly incompatible with the W hypothesis is achieved by requiring, instead, a cut on the transverse mass of the lepton-$\not\!\!E_{\rm T}$ system, as said above.

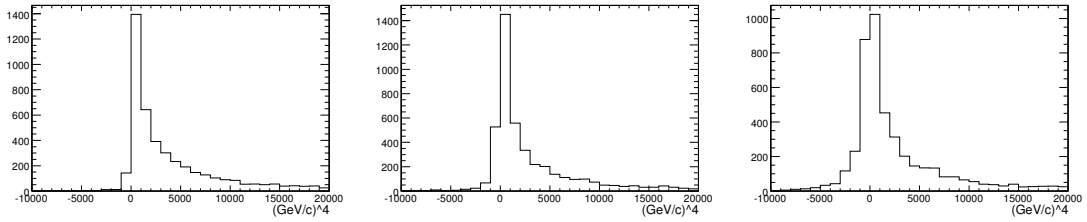

Figure 8: Discriminator Δ for signal events, as defined in Eq. 3, using the reconstructed lepton and the $\not\!\!E_{\rm T}$ defined as: (left) p_T of the true neutrino from W decay, (center) vectorial sum of all the invisible transverse momenta at generator level, (right) $\not\!\!E_{\rm T}$ used in the analysis, including detector effects, pile-up, etc.

It is estimated that with an integrated luminosity of 10 fb^{-1} the number of s-channel events surviving these cuts is 1010 ± 10 which should be compared to the background 5880 ± 70 t-channel, $(23.3 \pm 0.2) \times 10^3$ $t\bar{t}$, 160 ± 10 dileptonic Wt, 1150 ± 40 single-leptonic Wt, 1400 ± 35 $Wb\bar{b}$; the uncertainties quoted are only those due to the limited Monte Carlo statistics. Assuming equal efficiency for $Z(\rightarrow e^+e^-)b\bar{b}$ and $Z(\rightarrow \mu^+\mu^-)b\bar{b}$ (this is justified by the fact that these are roughly the same in all the other samples: 50%/50% e/μ for s- and t-channel single top, 48%/52% for $t\bar{t}$, 53%/47% $Wb\bar{b}$), and neglecting tau decays, 200 ± 90 $Zb\bar{b}$ events are estimated. Details on the effect of the preselection cuts on the considered samples are in Table 7 and 8.

A special consideration has to be given to the generic $W + jets$ background, since "$W + anything$" has a total cross section of 40 nb, huge with respect to all the processes considered so far. At the moment only a $W + 2j$ ($W \rightarrow e, \mu, \tau$) AlpGen sample has been used, where "$2j$" means that exactly two partons with $p_T >$ GeV/c and $-5 < \eta < +5$ are generated (of course additional jets may come from the showering). With this constraint, the cross section (times leptonic branching ratio) of the process is 2500 pb; the efficiency for the cuts described so far is $0.019 \pm 0.002\%$, resulting in 4750 ± 500 expected events. For consistency, also other $W + Nj$ samples should be used with the proper weights (the cross section for $W(\rightarrow e, \mu, \tau) + 0j$ is 30.000 pb, $W(\rightarrow e, \mu, \tau) + 1j$ 8.000 pb, $W(\rightarrow e, \mu, \tau) + 3j$ 722 pb, $W(\rightarrow e, \mu, \tau) + 4j$ 174 pb). This work is currently in progress and in the present note the study is limited to the $W + 2j$ sample, representing the main contribution.

As in Section 3.5, the multi-jet QCD contribution is neglected. This is justified by observing that the rejection factors calculated in Table 3 are then followed by the b-tagging of both jets (differently from the t-channel analysis, where only one b-tagging is required). One can have a rough idea of the supplementary rejection factor introduced by the double b-tagging by comparing the efficiencies for the $Wb\bar{b}$ and Wjj samples in Table 7 and 8. A more accurate estimation of the QCD background is ongoing.

4.3 Genetic Algorithm analysis

The following observables have been chosen in order to further discriminate between signal and background after preselection:

- the jet b-tagging discriminants;
- the jet transverse momenta (after "$\gamma - jet$" calibration);
- the mass of the reconstructed top;

Table 7: Efficiencies of the preselection cuts, with respect to the initial number of events, for the signal and the main backgrounds. Here $l = e, \mu, \tau$, and "HLT" includes the 1μ, $1e$ and $e \times j$ triggers.

Cut	s-ch. ($W \to l\nu$)	t-ch. ($W \to l\nu$)	$t\bar{t}$ (inclusive)	Wbb ($W \to l\nu$)
HLT and only $1l$	$37.5 \pm 0.2\%$	$42.5 \pm 0.1\%$	$30.1 \pm 0.1\%$	$29.4 \pm 0.1\%$
Isolation	$33.7 \pm 0.2\%$	$39.0 \pm 0.1\%$	$21.7 \pm 0.1\%$	$28.2 \pm 0.1\%$
$\not\!\!E_{\rm T}$ cut	$27.3 \pm 0.2\%$	$31.9 \pm 0.1\%$	$17.4 \pm 0.1\%$	$22.6 \pm 0.1\%$
M_T^W cut	$23.2 \pm 0.2\%$	$26.3 \pm 0.1\%$	$13.6 \pm 0.1\%$	$18.4 \pm 0.1\%$
$N_j \geq 2j$	$11.9 \pm 0.1\%$	$11.5 \pm 0.1\%$	$11.9 \pm 0.1\%$	$0.88 \pm 0.03\%$
$N_j = 2j$	$8.9 \pm 0.1\%$	$8.2 \pm 0.1\%$	$1.84 \pm 0.04\%$	$0.76 \pm 0.03\%$
b-tag	$3.07 \pm 0.07\%$	$0.72 \pm 0.02\%$	$0.28 \pm 0.02\%$	$0.14 \pm 0.01\%$

Table 8: Efficiencies of the preselection cuts, with respect to the initial number of events, for other backgrounds. Here $l = e, \mu, \tau$, and "HLT" includes the 1μ, $1e$ and $e \times j$ triggers. The Wjj sample is generated with (exactly) two partons with $p_T > 20$ GeV/c and $-5 < \eta < +5$ (this results in an indirect bias on the W spectrum, yielding an higher HLT efficiency with respect to $Wb\bar{b}$). The $Z(/\gamma^*)b\bar{b}$ sample is generated with $m(\mu^+\mu^-) > 5$ GeV/c^2.

Cut	Wt ($2\,W \to l\nu$)	Wt ($1\,W \to l\nu$)	Wjj ($W \to l\nu$)	$Z(/\gamma^*)b\bar{b}$ ($Z/\gamma^* \to \mu^+\mu^-$)
HLT and only $1l$	$36.66 \pm 0.15\%$	$46.5 \pm 0.1\%$	$40.40 \pm 0.07\%$	$8.3 \pm 0.1\%$
Isolation	$34.68 \pm 0.15\%$	$42.3 \pm 0.1\%$	$38.42 \pm 0.07\%$	$7.8 \pm 0.1\%$
$\not\!\!E_{\rm T}$ cut	$29.90 \pm 0.14\%$	$34.4 \pm 0.1\%$	$29.27 \pm 0.07\%$	$3.11 \pm 0.07\%$
M_T^W cut	$14.90 \pm 0.11\%$	$29.2 \pm 0.1\%$	$23.52 \pm 0.06\%$	$2.80 \pm 0.07\%$
$N_j \geq 2j$	$3.10 \pm 0.05\%$	$18.5 \pm 0.1\%$	$4.87 \pm 0.03\%$	$0.051 \pm 0.009\%$
$N_j = 2j$	$2.19 \pm 0.05\%$	$7.09 \pm 0.05\%$	$3.59 \pm 0.03\%$	$0.046 \pm 0.009\%$
b-tag	$0.24 \pm 0.02\%$	$0.34 \pm 0.01\%$	$0.019 \pm 0.002\%$	$0.008 \pm 0.004\%$

- the magnitude of the vectorial sum in the transverse plane of the momenta of the reconstructed top and of the remaining b-jet;
- the scalar sum of the transverse momenta of all the reconstructed objects, as defined in eq. 5.

The reconstructed top quark is formed by the W candidate reconstructed as described in the previous section, and one of the two b-jets, chosen according to the value of the "jet charge" (Q_j), defined as the sum of the charges of the tracks inside the jet cone, weighted over the projections of the track momenta along the jet axis. Since in t decay the W and the original b quark have opposite sign of the charge, the jet with Q_j "most opposite" to the W is used for top reconstruction. Table 9 shows a comparison with the more popular strategy of choosing the Wb pairing with the highest p_T.

Strategy	Good pairing	Wrong pairing
Highest-p_T top	56%	44%
Q_j most opposite to Q_l	67%	33%

Table 9: Comparison of the effectiveness of two different choice criteria for top reconstruction ($W - b$ pairing), in signal events. A "good pairing" is given by a distance $\Delta R < 0.5$ between the chosen jet and the b quark from top decay.

The distributions in Figures 9-12 show the events expected after preselection for 10 fb^{-1} integrated luminosity, taking into account the expected cross sections in the Standard Model for the signal and the considered backgrounds.

The cuts on these variables are optimized by means of the same genetic algorithm procedure described in Sec. 3.4. The surviving events after these cuts are shown in cascade in Table 10.

With this selection, after an integrated luminosity of 10 fb^{-1} one expects 273 ± 4 s-channel events surviving the cuts, as well as 630 ± 14 t-channel, 1260 ± 60 $t\bar{t}$, 3.5 ± 1.5 $Wt \to 2l$, 32 ± 15 $Wt \to 1l$, 155 ± 12 $Wb\bar{b}$ and $Wjj < 50$, giving $N_S/N_B \approx 0.13$.

4.4 Systematic uncertainties

The following sources of systematic uncertainty are considered:

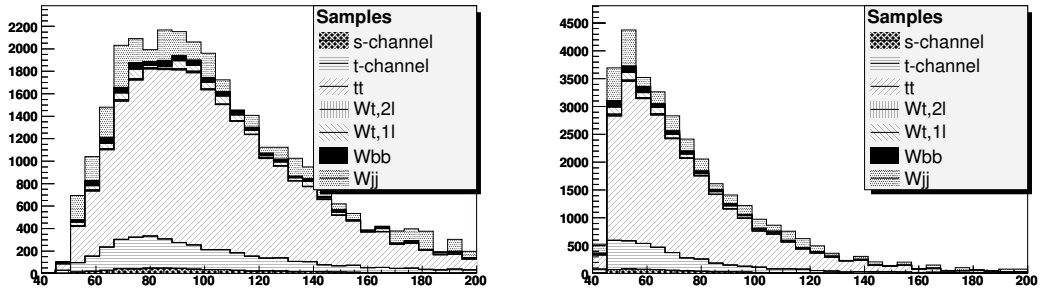

Figure 9: Transverse momentum distribution of the first (left) and second (right) jet in the event, with jets ordered in p_T and "$\gamma - jet$" calibrated.

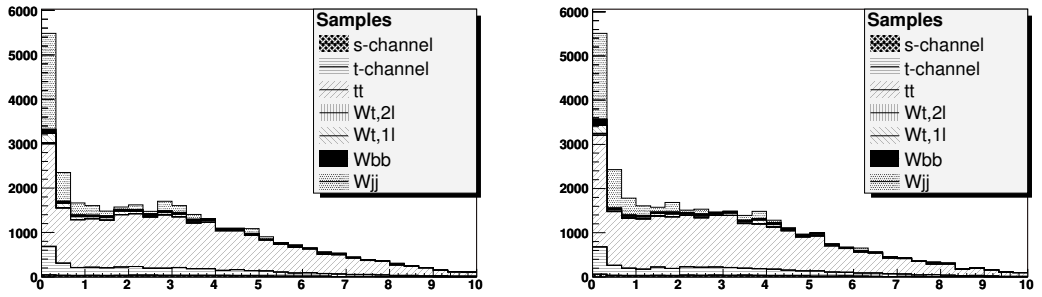

Figure 10: Distribution of the b-tagging discriminant of the first (left) and second (right) jet in the event, with jets ordered in p_T. No jet has negative values for the discriminant due to preselection, see Sec. 4.2.

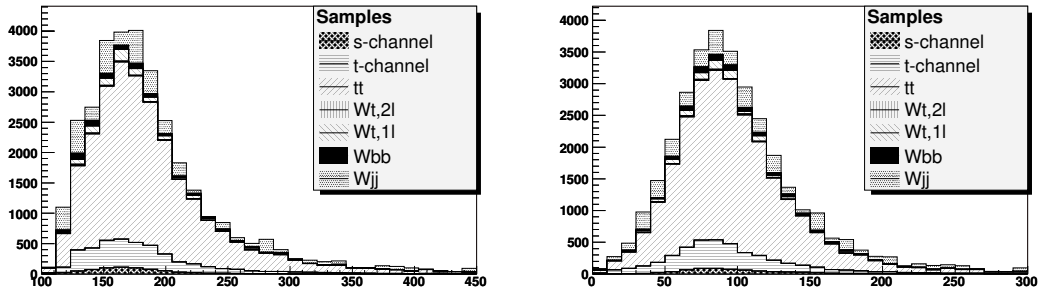

Figure 11: Invariant mass (left) and transverse momentum (right) distribution of the reconstructed top.

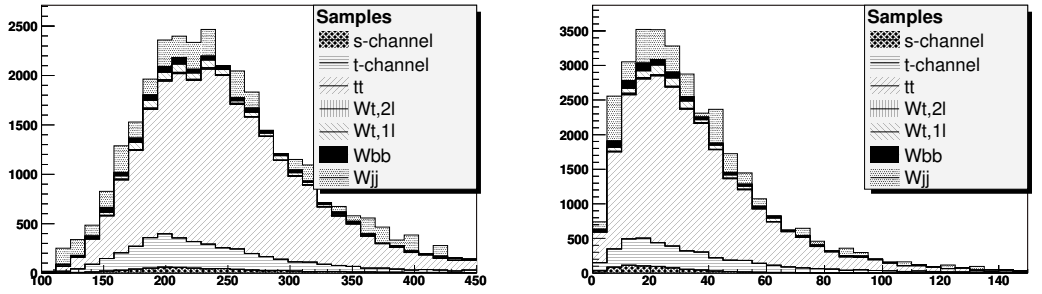

Figure 12: Distribution of the scalar (left) and of the vectorial (right) sum in the transverse plane of the momenta of the lepton, of the $\not{E}_{\mathrm{T}}$ and of the two b-jets.

- **Luminosity uncertainty.**

  The uncertainty due to luminosity is expected to be 5% [24].

Table 10: Final cuts and their efficiencies, with respect to the preselected samples, for the signal and the main backgrounds. Here $l = e, \mu, \tau$.

Cut	s-ch. ($W \to l\nu$)	t-ch. ($W \to l\nu$)	$t\bar{t}$ (inclusive)	Wbb ($W \to l\nu$)
b-tag(j_1)$>$ 0.4, b-tag(j_2)$>$ 0.1	85%	75%	78%	85%
$p_T(j_1) > 50$ GeV/c, $p_T(j_2) > 50$ GeV/c	68%	53%	70%	37%
$120 < M(l\nu b) < 220$ GeV/c^2	52%	34%	46%	26%
$25 < p_T(l\nu b) < 160$ GeV/c	48%	32%	43%	26%
$\Sigma_T < 20$ GeV/c	35%	15%	10.6%	12.5%
$H_T < 340$ GeV/c	27%	10.7%	5.4%	11.1%

- **Normalization uncertainty for background.**

  The theoretical errors to the total rates of the background samples are taken as 4% for the t-channel, 5% for $t\bar{t}$, 10% for Wt and 5% for $Wb\bar{b}$, corresponding to the theoretical uncertainties on the cross sections quoted in Table 1.

- **Jet Energy Scale (JES) uncertainty.**

  Using a calibration method based on $t\bar{t}$ events [29], the JES uncertainty after 10 fb^{-1} integrated luminosity is expected to be $\pm 5\%$ for jets with $p_T \approx 20$ GeV/c, and $\pm 2.5\%$ for $p_T > 50$ GeV/c. In the region between 20 and 50 GeV/c, a linear dependence $\delta p_T/p_T = [5 - \frac{1}{12}(p_T - 20 \text{ GeV}/c)]\%$ is assumed. This is a rough approximation of the true dependence.

  Rescaling the energy and momenta of the jets by those factors, a variation of $\pm 1.0\%$ is found on the efficiency for s-channel, $\pm 1.2\%$ for t-channel, $\pm 5.9\%$ for $t\bar{t}$ and $\pm 4.3\%$ for $Wb\bar{b}$. This systematic is positively correlated between single top s- and t-channel and $Wb\bar{b}$, and anti-correlated between these and $t\bar{t}$ (since an increase in the number of jets above the threshold gives a higher rejection factor for this background, and viceversa).

- **b-tagging identification uncertainty.**

  An uncertainty of $\pm 4\%$ is expected on the b-tagging efficiencies after 10 fb^{-1} [30]. Here this is translated to a $\pm 4\%$ uncertainty on the overall selection efficiencies, but work is ongoing for a better estimation.

- **Top mass, Parton Distribution Fuctions, Initial/Final State Radiation modelling.**

  For all these systematics sources, the procedure of error estimation was the following. A large sample of signal events has been generated through the complete chain and the dependence of the preselection efficiency (i.e. after the selection described in Section 4.2) for signal, ϵ_{presel}, as a function of $\hat{s}$ was obtained. Next, using only the event generator TopReX a statistically significant sample was generated with another set of parameters. Thus, the original preselection efficiency was reweighted according to the new $\hat{s}$ distribution. It is assumed here that these relative systematic uncertainties, determined for the preselection efficiency, hold as well for the final efficiency.

  - *Top mass.* The value of top quark mass was chosen to be m_{t} =175$\pm$2 GeV/c^2, where the central value is consistent with the Tevatron measurements and the variation is (conservatively) the uncertainty expected after the first 10 fb^{-1} of LHC data. One hundred of samples were generated with different values of m_{t} in this range. The obtained distribution is fitted with a Gaussian distribution to extract the systematic error on the choice of m_{t}.The relative systematic error on the selection efficiency corresponding to one standard deviation is equal to $\sigma^{m_{\text{t}}}_{\text{syst}}$=0.5% for the s-channel single top.
  - *Parton Distribution Fuctions.*

    To extract the dependence on the PDF uncertainty, two different PDF sets with their error sets were used: CTEQ61 (40 error sets) and CTEQ6M [31] The relative systematic error from the PDF choice is estimated, as above, as the RMS of the largest of the two distributions obtained for CTEQ61 and CTEQ6M. The result is $\sigma^{\text{PDF}}_{\text{syst}}$=0.7% for the s-channel single top.
  - *Initial/Final State Radiation modelling.*

    The procedure described in Ref. [34] was used to estimate the systematic uncertainty from the amount of initial and final states radiation. The model parameters were varied in the ranges Λ_{QCD}=0.25$\pm$0.1 GeV and Q^2_{max} from 0.25 to 4 GeV^2. The extreme values of the efficiencies are taken as systematic error: $\sigma^{\text{rad}}_{\text{syst}}$=0.5% for the s-channel single top.

Table 11: Number of selected events after 10 fb^{-1} and systematic uncertainties.

sample	selected	$\Delta\sigma$	JES	b-tag	M_{top}	PDF	ISR/FSR
S: s-channel	273	—	±3	±11	±1.5	±2	±1.5
B: t-channel	630	±25	±8	±25	—	—	—
B: $t\bar{t}$	1260	±63	±75	±50	—	—	—
B: $Wb\bar{b}$	155	±8	±7	±6	—	—	—

4.5 Background normalization

Table 11 shows that the systematic uncertainties on the number of $t\bar{t}$ selected events are quite large if compared to the number of signal events. This has a huge effect on the precision of the extracted cross section, as explained in Sec. 4.6.

In order to constrain the background, a control sample has to have the following properties:

1. the background process of interest is the vast majority of the selected sample (any contamination, including the signal, introduces a bias);
2. the selection is orthogonal to the main sample (in the sense that no event should enter both the main and the control sample);
3. the main systematic effects have roughly the same impact in the control sample as for the background events in the main sample.

The $t\bar{t}$ events in Table 11 are, in 41% of the cases, $t\bar{t} \to l^+\nu b l^-\bar{\nu}\bar{b}$ events with a lepton missed, and in the remaing cases $t\bar{t} \to l\nu b q\bar{q}'\bar{b}$ events with two jets missed ($t\bar{t} \to q\bar{q}'bq\bar{q}'\bar{b}$ events give a negligible contribution). These two categories of events are very differently affected by the Jet Energy Scale variation described in Sec. 4.4: in general, any variation going in the direction of more jets gives a better rejection of the $t\bar{t} \to l\nu b q\bar{q}'\bar{b}$ component with respect to the signal, while the $t\bar{t} \to l^+\nu b l^-\bar{\nu}\bar{b}$ events, having two quarks, are affected almost in the same way as the signal.

Here a selection is described for two control samples to be used to constrain the $t\bar{t}$ background and so reduce the impact of its uncertainties on our cross section measurement.

4.5.1 $t\bar{t} \to 2l + X$ enriched control sample

This sample is obtained by the same selection as in Sec. 4.2, with the only difference that instead of requiring one only lepton, two are required. They are taken of different flavours (i.e. one electron and one muon, in order to get rid of backgrounds with a Z) and of opposite sign, in order to reduce backgrounds where a $b \to l$ decay, or some other source of extra leptons, fake a $W \to l$ decay.

This selection is expected to yield, in 10 fb^{-1}, 7580 $t\bar{t}$ events, 107 Wt events, 3 WW events. Single top (t- and s-channel) contribution is expected to be negligible. By varying the Jet Energy Scale and the b-tagging efficiency as in Sec. 4.4, this total contamination of 110 events variates as $\pm4(JES) \pm 8(b-tag)$.

The selection efficiency for $t\bar{t} \to 2l$ events is found to be 0.822%. The ratio R_{c1} between the efficiencies in the main sample and in this control sample is $R_{c1} = 0.0681$, whose variations under JES and b-tagging efficiency systematic shifts are $\Delta R_{c1} = \pm0.0010(JES) \pm 0.0004(b-tag)$.

4.5.2 $t\bar{t} \to 1l + X$ enriched control sample

In this case the difference with respect to Sec. 4.2 is the request of three jets instead of two. Moreover, since statistics is very high and one of the main goals is to reduce as much as possible contaminations, only the muon channel is used, being cleaner than the electronic channel.

The result is a sample composition of 57.800 events in 10 fb^{-1}, with a contamination of 3270 $t\bar{t} \to 2l$, 1630 single top t-channel, 50 single top s-channel, 1000 Wt events, 850 $W + 3j$, 1040 $W + 4j$. By variating the Jet Energy Scale and the b-tagging efficiency as in Sec. 4.4, this total contamination of 7850 events variates as $\pm600(JES) \pm 50(b-tag)$.

The selection efficiency for $t\bar{t} \to 1l$ events is found to be 1.08%. The ratio R_{c2} between the efficiencies in the main sample and in this control sample is $R_{c2} = 0.0149$, whose variations under JES and b-tagging efficiency systematic shifts are $\Delta R_{c1} = \pm 0.0015(JES) \pm 0.0003(b-tag)$.

4.6 Results

N_S and N_B and their estimated uncertainties are listed in Table 11.

The cross section is extracted as

$$\sigma = \frac{N_{tot} - N_B}{\epsilon L}. \tag{11}$$

The statistical error is computed as

$$\frac{\Delta\sigma_{stat}}{\sigma} = \frac{\sqrt{N_S + N_B}}{N_S} = 18\%, \tag{12}$$

while the systematic error, without using the background normalization described in Sec. 4.5, is taken as

$$\frac{\Delta\sigma_{syst}}{\sigma} = \frac{\Delta N_S \oplus \Delta N_B}{N_S} = 44\%, \tag{13}$$

where ΔN_S and ΔN_B are the quadratic sums, for signal and backgrounds respectively, of the errors quoted in Table 11 (with the exception of the luminosity).

The total error, including also the 5% luminosity uncertainty, is

$$\frac{\Delta\sigma}{\sigma} = \frac{\Delta\sigma_{stat}}{\sigma} \oplus \frac{\Delta\sigma_{syst}}{\sigma} \oplus \frac{\Delta L}{L} = 48\%. \tag{14}$$

In order to use the information from the two control samples selected as in Sec. 4.5, Eq. 11 is rewritten as

$$\sigma = \frac{N_{tot} - b^0 - R_{c1}(N_{c1} - b^0_{c1}) - R_{c2}(N_{c2} - b^0_{c2})}{\epsilon L}, \tag{15}$$

where b^0 is the sum of the non-top backgrounds in the main sample, N_{c1} and N_{c2} are the total events selected in the two control regions, and b^0_{c1} and b^0_{c2} are their contaminations by non-top backgrounds, single top and other $t\bar{t}$ decays.

The corresponding relative systematic uncertainty is calculated as

$$\frac{\Delta\sigma_{syst}}{\sigma} = \left[\frac{\Delta R_{c1}}{R_{c1}} \oplus \frac{\sqrt{N_{c1}} \oplus \Delta b^0_{c1}}{N^{t\bar{t}\to 2l}_{c1}}\right] \times \frac{N^{t\bar{t}\to 2l}}{N_S} \oplus \left[\frac{\Delta R_{c2}}{R_{c2}} \oplus \frac{\sqrt{N_{c2}} \oplus \Delta b^0_{c2}}{N^{t\bar{t}\to 1l}_{c2}}\right] \times \frac{N^{t\bar{t}\to 1l}}{N_S} = 31\%, \tag{16}$$

where the largest contribution comes from $\frac{\Delta R_{c2}}{R_{c2}} = 10\%$, multiplied by $\frac{N^{t\bar{t}\to 1l}}{N_S} = 2.7$.

5 Conclusions and Outlook

Selection strategies are proposed for t-channel and s-channel single top production. Their effectiveness is shown taking into account the expected statistics after 10 fb^{-1}. This is the first analysis of single top events in CMS with a complete detector simulation.

Both analyses result to be dominated by systematic uncertainties, and after evaluation of the main systematic effects and of the main backgrounds the relative errors on the cross sections are expected to be

$$\frac{\Delta\sigma_t}{\sigma_t} = 2.7\%(stat) \oplus 8.1\%(syst) \oplus 5\%(lumi) = 9.9\%, \tag{17}$$

$$\frac{\Delta\sigma_s}{\sigma_s} = 18\%(stat) \oplus 31\%(syst) \oplus 5\%(lumi) = 36\%, \tag{18}$$

where for s-channel two control samples are used to constrain the $t\bar{t}$ uncertainty.

6 Acknowledgements

We would like to thank Joachim Mnich, Albert De Roeck, Jim Rohlf, Salavat Abdullin, Martin Gruenewald and Igor Golutvin for their comments and suggestions, and Olga Kodolova for her help on jet calibration issues.

This work is partly supported by RFBR 04-02-16476, RFBR 04-02-17448, Universities of Russia UR.02.02.503, and Russian Ministry of Education and Science NS.1685.2003.2 grants.

References

[1] I.I.Y. Bigi, Y.L. Dokshitzer, V.A. Khoze, J.H. Kuhn and P.M. Zerwas, Phys. Lett. B **181** (1986) 157.

[2] P. Nason, S. Dawson and R. K. Ellis, Nucl. Phys. B **303**, 607 (1988).

[3] S. Catani, M. L. Mangano, P. Nason and L. Trentadue, Nucl. Phys. B **478** (1996) 273 [arXiv:hep-ph/9604351].

[4] T. Stelzer, Z. Sullivan, and S. Willenbrock, Phys. Rev. D**56** (1997) 5919 [arXiv:hep-ph/9705398].

[5] M. C. Smith and S. Willenbrock, Phys. Rev. D **54** (1996) 6696 [arXiv:hep-ph/9604223].

[6] T. M. Tait, Phys. Rev. D **61** (2000) 034001 [arXiv:hep-ph/9909352];
A. Belyaev and E. Boos, Phys. Rev. D **63** (2001) 034012 [arXiv:hep-ph/0003260];
S. Zhu, Phys. Lett. B **524** (2002) 283 [Erratum-ibid. B **537** (2002) 351].

[7] E. E. Boos and A. V. Sherstnev, Phys. Lett. B **534** (2002) 97 [arXiv:hep-ph/0201271].

[8] E. Boos, L. Dudko, V. Savrin, CMS NOTE-2000/065; E. Boos, V. Bunichev, L. Dudko, V. Savrin, A. Sherstnev, Prepirnt SINP MSU 2005-16/782, to appear in Phys.Atom.Nucl.

[9] E. Boos *et al.* [CompHEP Collaboration], Nucl. Instrum. Meth. A **534**, 250 (2004) [arXiv:hep-ph/0403113].

[10] S. R. Slabospitsky and L. Sonnenschein, Comput. Phys. Commun. **148** (2002) 87 [arXiv:hep-ph/0201292].

[11] F. Maltoni and T. Stelzer, JHEP **0302** (2003) 027 [arXiv:hep-ph/0208156].

[12] T. Sjostrand, L. Lonnblad and S. Mrenna, [arXiv:hep-ph/0108264].

[13] CMS Coll., *Object oriented Simulation for CMS Analysis and Reconstruction*, Physics TDR Vol.I, Chapter 2,
OSCAR home page: http://cmsdoc.cern.ch/OSCAR/

[14] CMS Coll., *Object-oriented Reconstruction for CMS Analysis*, Physics TDR Vol.I, Chapter 2,
ORCA home page: http://cmsdoc.cern.ch/ORCA/

[15] CMS Coll., *FAMOS, FAst MOnte-Carlo Simulation*, Physics TDR Vol.I, Section 2.6.

[16] CMS Coll., Physics TDR Vol.I, Section 9.1.2.

[17] CMS Coll., Physics TDR Vol.I, Section 9.3.

[18] CMS Coll., Physics TDR Vol.I, Section 10.4.

[19] CMS Coll., Physics TDR Vol.I, Section 11.2.1.

[20] CMS Coll., Physics TDR Vol.I, Section 11.6.3.

[21] CMS Coll., Physics TDR Vol.I, Section 12.2.2.

[22] CMS collaboration, DAQ TDR.

[23] Z. Sullivan, Phys. Rev. D **70** (2004) 114012 [arXiv:hep-ph/0408049].

[24] CMS Coll., Physics TDR Vol.I, Chapter 8.

[25] T.M.P.Tait, C.-P.Yuan, Phys. Rev. D **63** (2001) 014018 [arXiv:hep-ph/0007298].

[26] S. Abdullin et al., *GARCON: Genetic Algorithm for Rectangular Cuts OptimizatioN. User's manual for version 2.0*, hep-ph/0605143, http://drozdets.home.cern.ch/drozdets/home/genetic/

[27] M. Beneke *et al.*, [arXiv:hep-ph/0003033].

[28] J. Campbell, R. K. Ellis and D. L. Rainwater, production Phys. Rev. D **68** (2003) 094021 [arXiv:hep-ph/0308195].

[29] CMS Coll., Physics TDR Vol.I, Section 11.6.5.

[30] CMS Coll., Physics TDR Vol.I, Section 12.2.8.

[31] J. Pumplin, D. R. Stump, J. Huston, H. L. Lai, P. Nadolsky and W. K. Tung, JHEP 0207 (2002) 012 [arXiv:hep-ph/0201195].

[32] A. D. Martin, R. G. Roberts, W. J. Stirling and R. S. Thorne, Eur. Phys. J. C 23 (2002) 73 [arXiv:hep-ph/0110215].

[33] S. Alekhin, Phys.Rev. D68 (2003) 014002 [arXiv:hep-ph/0211096].

[34] P. Bartalini, R. Chierici, A. De Roeck, CMS NOTE-2005/013.